2019 American Control Conference (ACC)
Philadelphia, PA, USA, July 10-12, 2019

Retroactivity Affects the Adaptive Robustness of Transcriptional Regulatory Networks

Junmin Wang[1] and Calin Belta[2]

Abstract— **Adaptation refers to the system's ability to respond transiently to an input signal and subsequently recover to the initial states. Adaptive robustness, the ability of a network to achieve adaptation, is subject to the loading effects arising from modular interconnections, known as retroactivity. Studying the effects of retroactivity on adaptive robustness facilitates the employment of retroactivity to improve circuit performance in synthetic biology. In this paper, we developed a framework for quantifying adaptive robustness via statistical model checking and used this framework to investigate the effects of retroactivity on adaptive robustness. We found that increasing retroactivity tends to raise adaptive robustness in networks where the output protein does not perform regulatory functions, such as incoherent feedforward loops.**

I. INTRODUCTION

Transcriptional regulatory networks (TRN) are collections of gene regulations that are mediated by transcriptional factors (TF). Variation in TRN contributes to diverse biological functions inside the cells. Adaptation is a biological function concerning the temporal dynamics of gene expression. It consists of a response phase, where the expression level of a gene responds transiently to an external stimulus, and a recovery phase, where the expression level adapts gradually to the initial value (Fig. 1) [1], [2]. Examples of adaptation include signal transduction [3], [4], [5], [6], bacteria chemotaxis [7], [8], [9], and homeostasis [10]. It is well known that TRN with certain topologies such as incoherent feedforward loops (IFFL) and negative feedback loops (NFBL) can mediate adaptations robustly. In other words, even though chemical kinetic rates vary significantly across a cell population, networks like IFFL are more likely to execute adaptations than most other networks. Many studies used the term adaptive robustness to describe the ability of a network to achieve adaptations regardless of the parameters [2], [11], [12]. In synthetic biology, investigating the adaptive robustness of various networks is especially important, as it is impossible to achieve precise control of chemical kinetic rates in synthetic TRN due to complex cellular environments. However, a standard quantitative definition of adaptive robustness has not been formalized.

One aim of synthetic biology is to facilitate and modulate biological functions via the engineering of synthetic TRN. Taking advantage of the high adaptive robustness of IFFL, researchers successfully constructed synthetic networks that can form biological patterns [13] or detect toxic chemical substances [14]. For improving circuit performance, a natural subsequent step is to investigate the effects of the parameters of IFFL on adaptations. Synthetic networks like IFFL are composed of transcriptional components, also known as modules. In the past, much attention was given to the effects of the parameters that are inherent in the modules, including protein production rates and decay rates [2], [11]. However, behaviors of networks are determined not only by behaviors of modules but also by the loading effects that arise from modular interconnections, known as retroactivity [15], [16]. Retroactivity refers to the phenomenon where transmitting a biological signal from the upstream system to the downstream system alters the behavior of the upstream system [17], [18], [12]. Based on theoretical foundations, the authors of [18] proved via experiments the existence of retroactivity in TRN and the feasibility of controlling retroactivity via plasmid copy numbers. According to [17] and [18], raising plasmid copy numbers and lowering protein production rates per plasmid by the same fold can increase the retroactivity of a system without affecting its steady states. Up till now retroactivity has been shown to impact biological functions including ultra-sensitivity [15], input-output characteristics [19], and response times [18], [20]. No previous work has yet been done on the effects of retroactivity on adaptive robustness. Understanding such effects will shed light on methods to control retroactivity and design synthetic circuits that can execute adaptations more robustly.

Our paper aims to study how retroactivity affects the adaptive robustness of different TRN. To facilitate such an investigation, we provided an explicit quantitative definition of adaptive robustness using Bounded Linear Temporal Logic (BLTL) and developed a framework for quantifying adaptive robustness via statistical model checking (SMC). We chose BLTL over Linear Temporal Logic because in practice, system simulations need to be finite in length [23]. The authors of [17] developed a systematic approach to constructing ordinary differential equation (ODE) models that account for retroactivity for a large class of TRN. Taking the approach shown in [17], we constructed two systems of ODE for TRN with and without retroactivity, and compared the robustness of these systems. We found that higher retroactivity generally brings stronger effects on adaptive robustness. In networks like IFFL, where the output protein does not perform regulatory functions, increasing retroactivity tends to increase adaptive robustness. Our findings imply that we can improve circuit performance by using retroactivity in advantageous

*This work was supported by the NSF under Grant No. CNS-1446607 and Grant No. CBET-0939511.

[1]J. Wang is with the Bioinformatics Graduate Program, Boston University, Boston, MA 02215, USA. Email: dawang@bu.edu

[2]C. Belta is with the Department of Mechanical Engineering, the Division of Systems Engineering, and the Bioinformatics Graduate Program, Boston University, Boston, MA 02215, USA. Email: cbelta@bu.edu

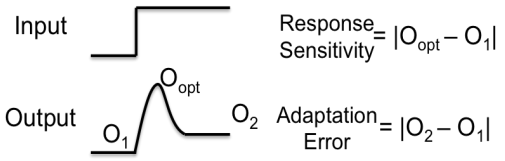

Fig. 1: Response sensitivity and adaptation errors.

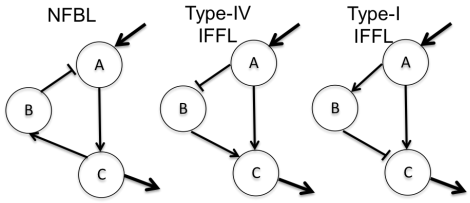

Fig. 2: Examples of three-node TRN. Arrows indicate activation, and edges with bars at the ends, inhibition. The leftmost network is an NFBL, in which the edges traversing B, A, and C accumulate in a negative regulation. The two networks on the right are IFFL, in which A directly activates C and indirectly represses C via B. In a type-IV IFFL, A represses B. In a type-I IFFL, A activates B.

ways.

The rest of this paper is organized into the following sections. In Section II, adaptive robustness is defined, and the problem we consider is formulated in a mathematical context. In Section III, ODE models with and without retroactivity are introduced. In Section IV, we demonstrate the application of SMC to our problem. A summary of our results follows in Section V.

II. PROBLEM FORMULATION

A. TRN and Adaptation

A TRN consisting of N genes can be represented by an N-node graph-like object, where each node is a gene (please refer to Fig. 2 for examples). There is a directed edge from node i to j if gene i regulates the expression of gene j. In this case, node i is also known as the parent of node j. The time evolution of a TRN is defined as a sequence of concentrations of proteins in the TRN, also known as a trajectory.

In this paper, we limited ourselves to TRN that contain three nodes. As was shown in several studies, a three-node TRN is a minimum network that facilitates adaptations, and a larger TRN can typically be reduced to a three-node TRN [11], [2]. We denote the three nodes by A, B, and C (Fig. 2). A is the input node activated by an external inducer. B is the node that transmits the signal from A to C. C is the output node, which is also the node of interest. Examples of three-node TRN are given in Fig. 2. Focusing on three-node TRN allowed us to conduct an exhaustive search of all possible network topologies.

Adaptation is a property concerning the time evolution of a network. Response sensitivity, defined as the difference between the output response and the initial value, quantifies the magnitude of biological pulses (Fig. 1). Networks capable of generating pulses can be used for gene therapy and the controlled delivery of drugs [21]. An adaptation error, defined as the difference between the initial value and the steady-state value post the induction, describes the ability of a system to homeostatically maintain its basal activity [22] (Fig. 1). An adaptation error equal to zero is termed perfect adaptation.

B. Specification and Adaptive Robustness

In this work, we used BLTL formulae over linear inequalities over concentrations of proteins to specify the functions of a network. A BLTL formula is built on a finite set of predicates over protein concentrations using Boolean operators: $\neg$ (negation), $\vee$ (disjunction), $\wedge$ (conjunction), $\Rightarrow$ (implication) and a temporal operator $\cup^k$ (until) with bound k [23]. More details about the syntax and the semantics of BLTL can be found in [23]. An example of a BLTL specification looks like:

$$\Phi_E = \left(x < 20 \cup^5 x = 20\right), \tag{1}$$

where x is the concentration of a protein. Φ_E means that the concentration of protein x should reach 20 within five time units and remain less than 20 at all preceding time units. Satisfaction of Φ_E by a trajectory σ is written as $\sigma \models \Phi_E$.

Assume the trajectory spans a time period of T. Let $\vec{x}$ denote the vector of protein concentrations of A, B, and C. The property of adaptation can be formally stated as:

$$\begin{aligned}\Phi = \Big(\Big(\dot{x}_C \geq 0 \cup^T \Big(\dot{x}_C < 0 \cup^T \Big(\dot{\vec{x}} = \vec{0}\Big)\Big)\Big) \vee \\ \Big(\dot{x}_C \leq 0 \cup^T \Big(\dot{x}_C > 0 \cup^T \Big(\dot{\vec{x}} = \vec{0}\Big)\Big)\Big)\Big) \wedge \underline{(s > s^*) \wedge (e < e^*)},\end{aligned} \tag{2}$$

where $\dot{x}_C$ represents the rate of change of concentration of C, and $\dot{\vec{x}}$, the vector that contains the rates of changes of all species' concentrations. s and e are response sensitivity and adaptation error; s^* and e^*, the corresponding thresholds.

Equation (2) can be separated into two parts: everything before the underlined and the underlined itself. The former requires that the concentration of C first respond to the initial stimuli either by rising or falling and then switch to recovery before the system eventually reaches the steady state. The latter excluds trajectories that have weak pulses or do not return to values that are close to the initial states.

We used Probabilistic BLTL (PBLTL) to specify the adaptive robustness of a TRN. The biochemical kinetic rates of the TRN are allowed to vary. A PBLTL formula that describes the ability of a network to achieve adaptations is expressed in the form $P_{\geq\theta}(\Phi)$, where Φ is the BLTL formula described in (2), and θ is a probability. A network satisfies the PBLTL formula if and only if a trajectory of the TRN satisfies the BLTL formula Φ in (2) with a probability greater than or equal to θ. We call θ the adaptive robustness of this network. A network is more robust than another if the former satisfies Φ with a higher probability than the latter.

The problem we considered is as follows: given a TRN and a BLTL formula Φ, compute the adaptive robustness of the TRN by calculating the probability θ with which the TRN satisfies the BLTL formula Φ. Solving this problem establishes a standard criterion for comparing different networks

and models. It provides us a framework for examining the effects of retroactivity on adaptive robustness of TRN.

III. Mathematical Models

In this section, we explain how we construct and simulate models for a TRN. In a TRN, the time evolution of any node i that is regulated by other node(s) and/or an external inducer can be described by the following ODE:

$$\dot{x_i} = f_i(x_i, \vec{y_i}), \tag{3}$$

where x_i and $\vec{y_i}$ represent the concentrations of node i and the parent(s) of node i, respectively. $\vec{y_i}$ includes the concentration of the external inducer if node i is regulated by an external inducer. f_i is expressed as:

$$f_i(x_i, \vec{y_i}) = H_i(\vec{y_i}) - \delta_i x_i, \tag{4}$$

where δ_i denotes the protein decay rate. $H_i(\vec{y_i})$ is the Hill function that describes the regulated production rate of x_i. Under the assumption of independent binding, $H_i(\vec{y_i})$ can be expressed as [17]:

$$H_i(\vec{y_i}) = \eta_i \frac{\pi_{i,0} + \sum_{X \subset \{1,2,...,m_i\}} \pi_{i,X} \prod_{j \in X} \left(\frac{y_{ij}}{K_{ij}}\right)^{h_{ij}}}{1 + \sum_{X \subset \{1,2,...,m_i\}} \prod_{j \in X} \left(\frac{y_{ij}}{K_{ij}}\right)^{h_{ij}}}, \tag{5}$$

where η_i stands for the total concentration of the promoter that expresses node i, and m_i is the number of parents of node i. Similar to [17], here we assume that no parents of the same node are identical. X corresponds to each complex formed by a different combination of TF; π_X denotes the production rate of the corresponding complex per plasmid ($\pi_{i,0}$ is the basal production rate, i.e., the production rate of the complex without parents); y_{ij}, h_{ij}, and K_{ij} represent the concentration, the Hill coefficient, and the dissociation constant of the j-th parent of node i. In this paper, we consider an AND logic for coregulation by multiple TF (a special case of independent binding), i.e., the regulated gene is turned on only when all the activators are abundant and all the repressors are scarce. An example of a Hill-function with the AND logic is given in Example 1.

Since a TRN is a collection of regulatory interactions among genes, the dynamics of a TRN can be described by:

$$\dot{\vec{x}} = f(\vec{x}), \tag{6}$$

where $\vec{x} = [x_1\ x_2\ ...\ x_N\ u]^T$, u is the concentration of the external inducer, and f is the collection of functions f_i ($i = 1, 2, ..., N$). We assume the inducer does not get produced or degraded, so the concentration of the inducer stays constant, i.e., $\dot{u} = 0$.

When retroactivity is considered, the equations describing the dynamics of a TRN change from (6) to:

$$\dot{\vec{x}} = [I + R(\vec{x})]^{-1} f(\vec{x}), \tag{7}$$

where $R(\vec{x})$ is known as the retroactivity matrix [17]. $R(\vec{x})$ can be calculated via the following equation [17]:

$$R(\vec{x}) = \sum_i V_i^T R_i(\vec{y_i}) V_i, \tag{8}$$

where V_i is binary, containing as many rows as the length of $\vec{y_i}$ and as many columns as the number of nodes in the network. The element in the j-th row and k-th column of V_i is 1 if the j-th parent of node i is node k, 0 otherwise. Under the assumption of independent binding, $R_i(\vec{y_i})$ is a diagonal matrix, where the k-th entry on the diagonal r_{ik} is [17]:

$$r_{ik} = \eta_i \frac{h_{ik}^2 y_{ik}^{h_{ik}-1}}{K_{ik}^{h_{ik}}} \left(1 + \left(\frac{y_{ik}}{K_{ik}}\right)^{h_{ik}}\right)^{-2}. \tag{9}$$

In (9), η_i stands for the total DNA concentration of node i. y_{ik}, h_{ik}, and K_{ik} are the protein concentration, the Hill coefficient, and the dissociation coefficient of the k-th parent of node i. It is easy to show that $V_i^T R_i(\vec{y_i}) V_i$ is always a diagonal matrix. Hence, $R(\vec{x})$ is also diagonal. More details about retroactivity, including its derivation can be found in [17].

A. Network Enumeration

Similar to [2], we first enumerated all possible topologies of three-node TRN. Each node in the network may interact with up to three nodes (two other nodes and itself). One node may activate, inhibit, or simply not regulate another node. There are altogether $3^9 = 19,683$ possible topologies, 3,645 of which have no direct or indirect links between the input A and the output C. We considered the remaining $16,038$ topologies in our study [2].

B. Network Simulation

To investigate the effects of retroactivity on adaptive robustness, we constructed and compared ODE models with and without retroactivity for each topology. To reduce the dimensions of parameter space, we normalized our models via methods shown in [24]. An example of normalization is given in Example 1. The normalized protein concentrations of A, B, and C, denoted by $\tilde{x}_A$, $\tilde{x}_B$, and $\tilde{x}_C$, are dimensionless and between values of 0 and 1. For simplicity of analysis, we assumed all normalized DNA concentrations have equal values denoted by $\tilde{\eta}$. For each enumerated topology, one ODE model without retroactivity and three models with retroactivity assuming $\tilde{\eta} = 0.1$, $\tilde{\eta} = 1$, and $\tilde{\eta} = 10$ were constructed. It is easy to see from (9) that as $\tilde{\eta}$ increases, the diagonal entries of the retroactivity matrices increase, giving rise to higher retroactivity.

We then generated trajectories by integrating the ODE. The initial states of A, B, and C were set to steady-state values of the networks with no induction. At t_0, the inducer's concentration x_I was changed from 0 to 10, maximally driving the expression of A (binding affinity K_{IA} was set to 0.4). The kinetic parameters were sampled uniformly from the same ranges of values used in [24]: $\tilde{K} \sim 0.001 - 1$ (sampled on the log scale), $h \sim 1 - 4$ (sampled on the linear scale), and $\delta \sim 0.01 - 1$ (sampled on the log scale).

Example 1: The topology of a type-IV IFFL is given in Fig. 2. We can describe the dynamics of a type-IV IFFL

without retroactivity via the following model:

$$\begin{aligned}
\frac{dx_A}{dt} &= f_A = \eta_A \frac{\pi_A \left(\frac{x_I}{K_{IA}}\right)^{h_{IA}}}{1+\left(\frac{x_I}{K_{IA}}\right)^{h_{IA}}} - \delta_A x_A \\
\frac{dx_B}{dt} &= f_B = \eta_B \frac{\pi_B}{1+\left(\frac{x_A}{K_{AB}}\right)^{h_{AB}}} - \delta_B x_B \\
\frac{dx_C}{dt} &= f_C = \eta_C \frac{\pi_C \left(\frac{x_A}{K_{AC}}\right)^{h_{AC}} \left(\frac{x_B}{K_{BC}}\right)^{h_{BC}}}{\left(1+\left(\frac{x_A}{K_{AC}}\right)^{h_{AC}}\right)\left(1+\left(\frac{x_B}{K_{BC}}\right)^{h_{BC}}\right)} \\
&\quad - \delta_C x_C .
\end{aligned} \tag{10}$$

With retroactivity, the dynamics can be described by:

$$\begin{bmatrix} \frac{dx_A}{dt} \\ \frac{dx_B}{dt} \\ \frac{dx_C}{dt} \end{bmatrix} = \begin{bmatrix} \frac{1}{1+b+a} & 0 & 0 \\ 0 & \frac{1}{1+c} & 0 \\ 0 & 0 & 1 \end{bmatrix} \begin{bmatrix} f_A \\ f_B \\ f_C \end{bmatrix}, \tag{11}$$

where

$$\begin{aligned}
a &= \eta_B \frac{h_{AB}^2 {x_A}^{h_{AB}-1}}{K_{AB}^{h_{AB}}} \left(1+\left(\frac{x_A}{K_{AB}}\right)^{h_{AB}}\right)^{-2} \\
b &= \eta_C \frac{h_{AC}^2 {x_A}^{h_{AC}-1}}{K_{AC}^{h_{AC}}} \left(1+\left(\frac{x_A}{K_{AC}}\right)^{h_{AC}}\right)^{-2} \\
c &= \eta_C \frac{h_{BC}^2 {x_B}^{h_{BC}-1}}{K_{BC}^{h_{BC}}} \left(1+\left(\frac{x_B}{K_{BC}}\right)^{h_{BC}}\right)^{-2} .
\end{aligned} \tag{12}$$

Following methods in [24], we let $\tilde{x}_A = \frac{x_A \delta_A}{\eta_A \pi_A}$, $\tilde{x}_B = \frac{x_B \delta_B}{\eta_B \pi_B}$, $\tilde{x}_C = \frac{x_C \delta_C}{\eta_C \pi_C}$, $\tilde{K}_{AB} = \frac{K_{AB} \delta_A}{\eta_A \pi_A}$, $\tilde{K}_{AC} = \frac{K_{AC} \delta_A}{\eta_A \pi_A}$, and $\tilde{K}_{BC} = \frac{K_{BC} \delta_B}{\eta_B \pi_B}$. The model without retroactivity shown in (10) is normalized to:

$$\begin{aligned}
\frac{d\tilde{x}_A}{dt} &= f_{\tilde{A}} = \delta_A \left(\frac{\left(\frac{x_I}{K_{IA}}\right)^{h_{IA}}}{1+\left(\frac{x_I}{K_{IA}}\right)^{h_{IA}}} - \tilde{x}_A \right) \\
\frac{d\tilde{x}_B}{dt} &= f_{\tilde{B}} = \delta_B \left(\frac{1}{1+\left(\frac{\tilde{x}_A}{\tilde{K}_{AB}}\right)^{h_{AB}}} - \tilde{x}_B \right) \\
\frac{d\tilde{x}_C}{dt} &= f_{\tilde{C}} = \delta_C \left(\frac{\left(\frac{\tilde{x}_A}{\tilde{K}_{AC}}\right)^{h_{AC}} \left(\frac{\tilde{x}_B}{\tilde{K}_{BC}}\right)^{h_{BC}}}{\left(1+\left(\frac{\tilde{x}_A}{\tilde{K}_{AC}}\right)^{h_{AC}}\right)\left(1+\left(\frac{\tilde{x}_B}{\tilde{K}_{BC}}\right)^{h_{BC}}\right)} \right. \\
&\quad \left. -\tilde{x}_C \right) .
\end{aligned} \tag{13}$$

Then we let $\tilde{\eta}_{AB} = \frac{\eta_B}{K_{AB}}$, $\tilde{\eta}_{AC} = \frac{\eta_C}{K_{AC}}$, and $\tilde{\eta}_{BC} = \frac{\eta_C}{K_{BC}}$. The model with retroactivity shown in (11) is normalized to:

$$\begin{bmatrix} \frac{d\tilde{x}_A}{dt} \\ \frac{d\tilde{x}_B}{dt} \\ \frac{d\tilde{x}_C}{dt} \end{bmatrix} = \begin{bmatrix} \frac{1}{1+\tilde{b}+\tilde{a}} & 0 & 0 \\ 0 & \frac{1}{1+\tilde{c}} & 0 \\ 0 & 0 & 1 \end{bmatrix} \begin{bmatrix} f_{\tilde{A}} \\ f_{\tilde{B}} \\ f_{\tilde{C}} \end{bmatrix}, \tag{14}$$

where

$$\begin{aligned}
\tilde{a} &= \tilde{\eta}_{AB} h_{AB}^2 \left(\frac{\tilde{x}_A}{\tilde{K}_{AB}}\right)^{h_{AB}-1} \left(1+\left(\frac{\tilde{x}_A}{\tilde{K}_{AB}}\right)^{h_{AB}}\right)^{-2} \\
\tilde{b} &= \tilde{\eta}_{AC} h_{AC}^2 \left(\frac{\tilde{x}_A}{\tilde{K}_{AC}}\right)^{h_{AC}-1} \left(1+\left(\frac{\tilde{x}_A}{\tilde{K}_{AC}}\right)^{h_{AC}}\right)^{-2} \\
\tilde{c} &= \tilde{\eta}_{BC} h_{BC}^2 \left(\frac{\tilde{x}_B}{\tilde{K}_{BC}}\right)^{h_{BC}-1} \left(1+\left(\frac{\tilde{x}_B}{\tilde{K}_{BC}}\right)^{h_{BC}}\right)^{-2} .
\end{aligned} \tag{15}$$

Based on our assumption of equal normalized DNA concentrations, $\tilde{\eta}_{AB} = \tilde{\eta}_{AC} = \tilde{\eta}_{BC} = \tilde{\eta}$.

IV. Statistical Analysis

In this section, we provide solutions to the problem formulated in Section II.

A. Bayesian Interval Estimation

The authors of [23] presented an algorithm for estimating the Bayesian interval that contains the true probability of adaptation with an arbitrarily high probability. The algorithm samples trajectories from a stochastic system iteratively and checks each trajectory against the specification. At each stage, the posterior mean, which is the Bayes estimator for the probability, is updated. The algorithm terminates and returns the probability estimate upon achieving the coverage goal. The estimate is in the form of a Bayesian confidence interval. Otherwise, the algorithm continues by sampling another trajectory.

We used the above algorithm to estimate the probability that a random execution trace of the TRN satisfies the property of adaptation specified by a BLTL formula. Due to practical concerns of simulation times, the BLTL formula we implemented differs slightly from (2) and is specified as follows:

$$\begin{aligned}
\Phi = &\left(\left(\dot{\tilde{x}}_C \geq 0 \cup^{10000} \left(\dot{\tilde{x}}_C < 0 \cup^{10000} \left(||\dot{\vec{\tilde{x}}}||_\infty \leq 10^{-4}\right)\right)\right) \vee \right. \\
&\left. \left(\dot{\tilde{x}}_C \leq 0 \cup^{10000} \left(\dot{\tilde{x}}_C > 0 \cup^{10000} \left(||\dot{\vec{\tilde{x}}}||_\infty \leq 10^{-4}\right)\right)\right)\right) \wedge \\
&(s > 0.1) \wedge (e < 0.01) .
\end{aligned} \tag{16}$$

In (16), $\dot{\tilde{x}}_C$ represents the rate of change of the normalized concentration of C, and $||\dot{\vec{\tilde{x}}}||_\infty$ the infinity norm of the vector containing the rates of changes of all normalized species' concentrations. The maximum simulation duration is set to 10,000, and the thresholds on the response sensitivity and the adaptation error are set to 0.1 and 0.01 (we experimented with other cut-off values and arrived at the same conclusions). We defined our BLTL specification such that networks that spend too much time approaching steady states or have oscillatory behaviors were excluded. For the algorithm, a beta prior with $\alpha = \beta = 1$ was used. For the algorithm parameters, half interval size δ was set to 0.01, and coverage goal c was set to 0.99. Explanations of the algorithm parameters can be found in [23]. The probability estimate the algorithm returns, $\hat{\theta}$, is the adaptive robustness of the network.

Our simulations suggest that the type-IV IFFL (Fig. 2) has the highest adaptive robustness among all models without retroactivity, 0.5480. This means that the unknown probability θ that a type-IV IFFL achieves adaptation lies in $[0.5480 - 0.01, 0.5480 + 0.01]$ with probability $1 - \frac{(1-0.99)\times 0.02}{0.99\times 0.98}$, if retroactivity is not considered.

Here we consider a network model to be adaptive if its adaptive robustness exceeds 0.05 without retroactivity. There are altogether 71 adaptive networks, the adaptive robustness of which, with and without retroactivity, was compared. As is suggested by Fig. 3, higher retroactivity in general brings

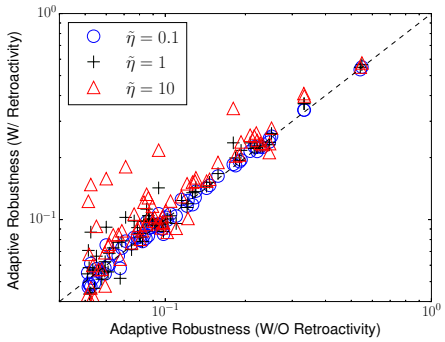

Fig. 3: Adaptive robustness of adaptive networks. X-axis represents models without retroactivity, and Y-axis, the counterparts with retroactivity. Blue circles represent models assuming $\tilde{\eta} = 0.1$, black pluses, models assuming $\tilde{\eta} = 1$, and red triangles, models assuming $\tilde{\eta} = 10$. The black dashed line corresponds to equal adaptive robustness.

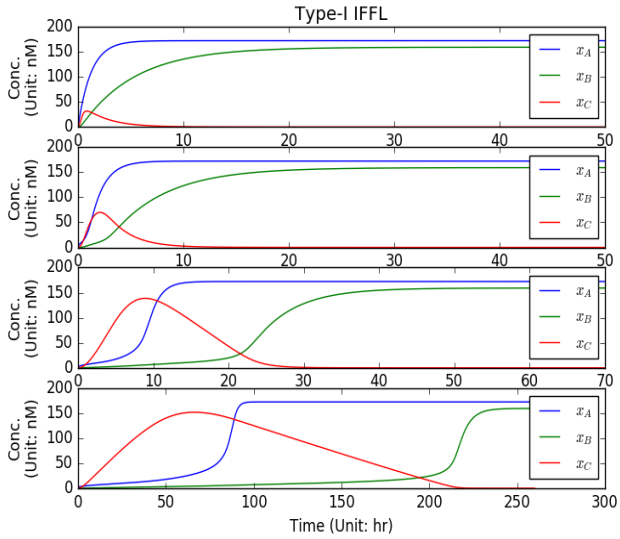

Fig. 4: An example of trajectories simulated by non-normalized type-I IFFL models. Values of the parameters are: $K_{IA} = 0.4$nM, $K_{AB} = 24.62$nM, $K_{AC} = 10$nM, $K_{BC} = 10$nM, $h_{IA} = 1$, $h_{AB} = 2.60$, $h_{AC} = 3.28$, $h_{BC} = 2.77$, $\delta_A = 0.81\text{hr}^{-1}$, $\delta_B = 0.20\text{hr}^{-1}$, $\delta_C = 0.47\text{hr}^{-1}$. DNA concentrations increase and protein production rates per plasmid decrease from the top figure to the bottom figure. For fair comparison, the products of DNA concentrations and protein production rates per plasmid are kept fixed. Top: $\pi_A\eta_A = 144.18\text{nM} \cdot \text{hr}^{-1}$, $\pi_B\eta_B = 31.29\text{nM} \cdot \text{hr}^{-1}$, $\pi_C\eta_C = 80\text{nM} \cdot \text{hr}^{-1}$; 2nd from the top: $\pi_A = 58.61\text{hr}^{-1}$, $\pi_B = 12.72\text{hr}^{-1}$, $\pi_C = 80\text{hr}^{-1}$, $\eta_A = 2.46$nM, $\eta_B = 2.46$nM, $\eta_C = 1$nM; 2nd from the bottom: $\pi_A = 5.86\text{hr}^{-1}$, $\pi_B = 1.27\text{hr}^{-1}$, $\pi_C = 8\text{hr}^{-1}$, $\eta_A = 24.6$nM, $\eta_B = 24.6$nM, $\eta_C = 10$nM; bottom: $\pi_A = 0.59\text{hr}^{-1}$, $\pi_B = 0.13\text{hr}^{-1}$, $\pi_C = 0.8\text{hr}^{-1}$, $\eta_A = 246$nM, $\eta_B = 246$nM, $\eta_C = 100$nM. When normalized, the four models from the top to the bottom represent no retroactivity, $\tilde{\eta} = 0.1$, $\tilde{\eta} = 1$, and $\tilde{\eta} = 10$. All parameters are within reasonable ranges of biological parameters given in [17].

about stronger effects on adaptive robustness, as red pluses ($\tilde{\eta} = 0.1$) are on average more distant from the reference line than blue diamonds ($\tilde{\eta} = 1$), and black circles ($\tilde{\eta} = 10$) more distant than red pluses.

B. Parameter Perturbation

The data points in Fig. 3 are scattered on both sides of the reference line. This observation suggests that increasing retroactivity can either enhance or reduce adaptive robustness depending on the circuit topologies. To investigate the mixed effects of retroactivity on adaptive robustness, we performed a parameter perturbation analysis. Specifically, we randomly selected 100 parameters that facilitate adaptations in models without retroactivity. Keeping these parameters fixed, we set $\tilde{\eta}$ to 0.1, 1, and 10 and simulated the counterpart models with retroactivity. The perturbation analysis was performed on type-IV IFFL and type-I IFFL (Fig. 2). These two motifs are chosen because they have the overall highest adaptive robustness among all network motifs, with and without retroactivity. The average response sensitivity and adaptation errors calculated for each model are shown in Table I, which suggests that increasing $\tilde{\eta}$ enhances response sensitivity in IFFL networks. The underlying causes are rooted in the retroactivity matrices. Since IFFL networks differ merely in the types of regulation, the retroactivity matrix given in (14) and (15) is the same for all IFFL. From (14), it is easy to see that increasing $\tilde{\eta}$ decreases $\dot{\tilde{x}}_A$ and $\dot{\tilde{x}}_B$, i.e., changes of protein concentrations of both A and B become slower (Fig. 4). Inhibition of B by A takes a longer time till B reaches a sufficiently low concentration such that B can no longer activate C. Simultaneously, $\tilde{\eta}$ does not affect $\dot{\tilde{x}}_C$. Consequently, C accumulates a larger response since $\dot{\tilde{x}}_C$ is unaffected by $\tilde{\eta}$, and the growth time of $\tilde{x}_C$ becomes longer. Higher response sensitivity can lead to higher adaptive robustness as a trajectory becomes more likely to satisfy (16).

Our analysis above can be generalized to other network topologies. It is easy to prove that if C is not a regulator in a network, the bottom right entry of $R(\vec{x})$ in (8) is always 0. In these networks, the rate of change of C is not slowed down by retroactivity. Increasing DNA concentrations enhances response sensitivity in these networks, leading to higher adaptive robustness. We found that higher retroactivity increases adaptive robustness consistently in 74 networks, the three most frequent motifs of which are IFFL, NFBL between A and B, and negative self-feedback loops on B. A common feature of these motifs is that C is not a regulator, which confirms our hypothesis.

One direct biological implication of our findings is that changing plasmid copy numbers can enhance adaptive robustness. One approach to increasing retroactivity while keeping the steady-state behavior of the network unchanged is to raise the plasmid copy number and lower the protein

TABLE I: Results from the perturbation analysis. Mean response sensitivity and adaptation errors calculated from 100 randomly selected parameter sets are shown in the 2nd and 3rd columns. The adaptive robustness of these networks inferred earlier via the algorithm shown in [23] is listed in the last columns.

Type-IV IFFL			
$\tilde{\eta}$	Response	Error	Robustness
N/A	0.6602	3.7×10^{-4}	0.5480
0.1	0.6625	3.7×10^{-4}	0.5497
1	0.6712	3.7×10^{-4}	0.5648
10	0.6935	3.7×10^{-4}	0.5758

Type-I IFFL			
$\tilde{\eta}$	Response	Error	Robustness
N/A	0.3831	1.6×10^{-3}	0.1800
0.1	0.4027	1.6×10^{-3}	0.1854
1	0.5052	1.6×10^{-3}	0.2357
10	0.7184	1.6×10^{-3}	0.3463

production rate per plasmid by the same fold. An example of such an approach is given in Fig. 4, where the plasmid copy number and the protein production rate per plasmid are allowed to vary, but the total protein production rate is kept fixed. It is clear from Fig. 4 that A and B maintain the same steady states, whereas C accumulates different levels of response due to different degrees of retroactivity. Experiment-wise, plasmid copy number can be raised via an increase in plasmid dose, and protein production rate per plasmid can be lowered by methods such as adding nucleotides between the promoter and the transcription start site.

V. CONCLUSIONS

We developed a framework for inferring adaptive robustness via SMC and used our framework to study the effects of retroactivity on adaptive robustness. We found that in networks where the output is not a regulator, such as IFFL, increasing retroactivity enhances adaptive robustness. Note, that our framework can be applied to study the effects of retroactivity on the robustness of other biological functions.

From a circuit design perspective, our work provides a novel insight into a common problem of choice in synthetic biology: whether to use a high plasmid dose of a weak promoter or a low plasmid dose of a strong promoter to drive gene expression. While neither choice may affect the overall protein production rate, the former choice brings about a higher degree of retroactivity than the latter. Our findings suggest that appropriate choices of promoters and plasmid doses can improve the adaptive robustness of synthetic TRN.

REFERENCES

[1] U. Alon, *An Introduction to Systems Biology - Design Principles of Biological Circuits*. Chapman and Hall, 2007.

[2] W. Shi, W. Ma, L. Xiong, M. Zhang, and C. Tang, "Adaptation with transcriptional regulation," *Sci. Rep.*, vol. 7, p. 42648, 2017.

[3] M. Behar, N. Hao, H. G. Dohlman, and T. C. Elston, "Mathematical and computational analysis of adaptation via feedback inhibition in signal transduction pathways," *Biophys. J.*, vol. 93, no. 3, pp. 806–821, 2007.

[4] M. Cohen, A. Kicheva, A. Ribeiro, R. Blassberg, K. M. Page, C. P. Barnes, and J. Briscoe, "Ptch1 and gli regulate shh signalling dynamics via multiple mechanisms," *Nat. Commun.*, vol. 6, p. 6709, 2015.

[5] K. Takeda, D. Shao, M. Adler, P. G. Charest, W. F. Loomis, H. Levine, A. Groisman, W.-J. Rappel, and R. A. Firtel, "Incoherent feedforward control governs adaptation of activated ras in a eukaryotic chemotaxis pathway," *Sci. Signal.*, vol. 5, no. 205, 2012.

[6] D. Muzzey, C. A. Gómez-Uribe, J. T. Mettetal, and A. van Oudenaarden, "A systems-level analysis of perfect adaptation in yeast osmoregulation," *Cell*, vol. 138, no. 1, pp. 160–171, 2009.

[7] U. Alon, M. G. Surette, N. Barkai, and S. Leibler, "Robustness in bacterial chemotaxis," *Nature*, vol. 397, no. 6715, pp. 168–171, 1999.

[8] N. Barkai and S. Leibler, "Robustness in simple biochemical networks," *Nature*, vol. 387, p. 913, 1997.

[9] R. M. Macnab and D. E. Koshland, "The gradient-sensing mechanism in bacterial chemotaxis," *Proc. Natl. Acad. Sci. U.S.A.*, vol. 69, no. 9, pp. 2509–2512, 1972.

[10] H. El-Samad, J. P. Goff, and M. Khammash, "Calcium homeostasis and parturient hypocalcemia: an integral feedback perspective," *J. Theor. Biol.*, vol. 214, no. 1, pp. 17–29, 2002.

[11] W. Ma, A. Trusina, H. El-Samad, W. A. Lim, and C. Tang, "Defining network topologies that can achieve biochemical adaptation." *Cell*, vol. 138, no. 4, pp. 760–773, 2009.

[12] S. Mou and D. D. Vecchio, "How retroactivity impacts the robustness of genetic networks," in *Proc. IEEE Conf. Decis. Control*, 2015, pp. 1551–1556.

[13] S. Basu, Y. Gerchman, C. Collins, F. Arnold, and R. Weiss, "A synthetic multicellular system for programmed pattern formation," *Nature*, vol. 434, pp. 1130–34, 2005.

[14] F. Barone, F. Dorr, L. E. Marasco, S. Mildiner, I. L. Patop, S. Sosa, L. G. Vattino, F. A. Vignale, E. Altszyler, B. Basanta, N. Carlotto, J. Gasulla, M. Giménez, A. Grande, N. Nieto Moreno, H. R. Bonomi, and A. D. Nadra, "Design and evaluation of an incoherent feed-forward loop for an arsenic biosensor based on standard igem parts," *Synth. Biol.*, vol. 2, no. 1, 2017.

[15] A. C. Ventura, P. Jiang, L. Van Wassenhove, D. Del Vecchio, S. D. Merajver, and A. J. Ninfa, "Signaling properties of a covalent modification cycle are altered by a downstream target." *Proc. Natl. Acad. Sci. U.S.A.*, vol. 107, no. 22, pp. 10 032–10 037, 2010.

[16] D. Del Vecchio, A. J. Ninfa, and E. D. Sontag, "Modular cell biology: retroactivity and insulation," *Mol. Syst. Biol.*, vol. 4, p. 161, 2008.

[17] A. Gyorgy and D. D. Vecchio, "Modular composition of gene transcription networks," *PLOS Comput. Biol.*, 2014.

[18] S. Jayanthi, K. S. Nilgiriwala, and D. Del Vecchio, "Retroactivity controls the temporal dynamics of gene transcription," *ACS Synth. Biol.*, vol. 2, no. 8, pp. 431–441, 2013.

[19] R. C. Brewster, F. M. Weinert, H. G. Garcia, D. Song, M. Rydenfelt, and R. Phillips, "The transcription factor titration effect dictates level of gene expression." *Cell*, vol. 156, no. 6, pp. 1312–1323, 2014.

[20] P. Jiang, A. C. Ventura, E. D. Sontag, S. D. Merajver, A. J. Ninfa, and D. Del Vecchio, "Load-induced modulation of signal transduction networks," *Sci. Signal.*, vol. 4, no. 194, 2011.

[21] A. S. Khalil and J. J. Collins, "Synthetic biology: applications come of age," *Nat. Rev. Genet.*, vol. 11, no. 5, pp. 367–379, 05 2010.

[22] J. E. Ferrell, "Perfect and near-perfect adaptation in cell signaling," *Cell Systems*, vol. 2, no. 2, pp. 62–67, 2016.

[23] P. Zuliani, A. Platzer, and E. M. Clarke, "Bayesian statistical model checking with application to stateflow/simulink verification," *Form. Methods Syst. Des.*, vol. 43, no. 2, pp. 338–367, 2013.

[24] L.-H. Cao, B.-Y. Jing, D. Yang, X. Zeng, Y. Shen, Y. Tu, and D.-G. Luo, "Distinct signaling of drosophila chemoreceptors in olfactory sensory neurons," *Proc. Natl. Acad. Sci. U.S.A*, vol. 113, no. 7, pp. 902–911, 2016.